CHEMISTRY

Practical water production from desert air

Farhad Fathieh[1]*, Markus J. Kalmutzki[1,2]*, Eugene A. Kapustin[1,2]*, Peter J. Waller[1,2], Jingjing Yang[1,2], Omar M. Yaghi[1,2,3]†

Energy-efficient production of water from desert air has not been developed. A proof-of-concept device for harvesting water at low relative humidity was reported; however, it used external cooling and was not desert-tested. We report a laboratory-to-desert experiment where a prototype using up to 1.2 kg of metal-organic framework (MOF)–801 was tested in the laboratory and later in the desert of Arizona, USA. It produced 100 g of water per kilogram of MOF-801 per day-and-night cycle, using only natural cooling and ambient sunlight as a source of energy. We also report an aluminum-based MOF-303, which delivers more than twice the amount of water. The desert experiment uncovered key parameters pertaining to the energy, material, and air requirements for efficient production of water from desert air, even at a subzero dew point.

INTRODUCTION

About 13 sextillion (10^{21}) liters of water exist in the atmosphere at any given time (*1*). This is a recyclable natural resource with potential to water the arid regions of the world. Methods to harvest water from humid air are known (*2*–*6*), but doing so at low humidity in desert climates is as yet undeveloped (*7*). The difficulty in establishing a practical water harvesting cycle (WHC; Fig. 1) for low-humidity climates is twofold: finding a material capable of facile water capture and release (capture cycle) and providing sufficient cooling energy such that the temperature of the condenser is lower than that of the released water vapor to allow for liquid water formation (collecting cycle). Although the two cycles have been shown to work with intensive energy input (*8*), it remains unknown whether they can produce water under natural cooling with energy only from ambient sunlight.

Water uptake in metal-organic frameworks (MOFs) has been reported (*7*, *9*–*14*), and a recent proof-of-concept device based on these materials showed encouraging results (*15*). However, this device (i) used an additional source of cooling, (ii) yielded water droplets but not of sufficient quantity to be collected, (iii) required a copper mesh to provide structural rigidity and heat transfer, and (iv) was not tested in the desert. To bring this advance into practice, we address here all these issues in a new design tested in the laboratory and the desert of Arizona, USA. This laboratory-to-desert study uncovered critical parameters concerning the interplay between water release, condensation, and material properties and consequently led to water production under natural cooling and ambient sunlight, with no additional energy input. We show that 0.550 kg of MOF-801 can be implemented into a device to produce up to 78 g of water per day-and-night cycle under laboratory conditions and 55 g in Arizona under natural cooling and ambient sunlight at 5 to 40% of relative humidity (RH). In addition, 0.450 kg of our newly designed MOF-303 produced up to 105 g of water under laboratory conditions, thus bringing water production at low humidity a step closer to practical use.

[1]Department of Chemistry, Kavli Energy NanoScience Institute, and Berkeley Global Science Institute, University of California, Berkeley, Berkeley, CA 94720, USA. [2]Materials Sciences Division, Lawrence Berkeley National Laboratory, Berkeley, CA 94720, USA. [3]King Abdulaziz City for Science and Technology (KACST), Riyadh 11442, Saudi Arabia.
*These authors contributed equally to this work.
†Corresponding author. Email: yaghi@berkeley.edu

RESULTS AND DISCUSSION

Energy, materials, and air requirements for the WHC

Our considerations in the design of the water production system took into account the energy, materials, and air requirements for the WHC. Figure 1A shows that the capture cycle starts with saturation of unsaturated MOF upon exposure to desert air at nighttime. This is followed by the release of captured water from the saturated MOF upon exposure to sunlight during daytime. The collecting cycle takes place during daytime when the released water vapor humidifies the air in the vicinity of the MOF. The hot humid air is subsequently cooled down, in our case by ambient cooling, to its dew point, resulting in liquefied water at the condenser. The collecting cycle (release-condensation) continues until the end of the daytime when the liquid water is collected and the next WHC starts.

The saturation of the MOF is determined by the extent to which water fills the pores. This quantity is the water capture capacity (ω_{cap}: captured water per mass of MOF) at a given RH, and it can be estimated from the water adsorption isotherm. Large values of ω_{cap} at low RH can be achieved in hydrolytically stable MOFs with large pore volumes and hydrophilic pore environments. In addition to the MOF's sorption properties, a design optimizing the packing porosity is needed to enhance the intercrystalline diffusion and reach ω_{cap} within the 14 to 16 hours of nighttime.

The energy absorbed by the MOF is spent on three different processes: overcoming the MOF-water interactions ($q_{H,\ latent} = \omega_{cap} q_{st}$), increasing the temperature of the MOF ($q_{H,sensible}$), and dissipating due to heat loss ($q_{H,loss}$). Considering $q_{H,sensible} \ll q_{H,latent}$ for MOFs and $q_{H,loss} \ll q_{H,sensible}$ for a thermally insulated adsorbent container, the majority of the absorbed energy is spent on breaking the MOF-water interactions to release water, and therefore, a MOF with low isosteric heat of adsorption (q_{st}) is desirable. A practical capture cycle with maximized water release should follow inequality (Eq. 1), where we consider the minimum solar energy ($q_{H,min}$) that allows the release of the entire amount of captured water (see section S9).

The performance of the capture cycle can be evaluated by the release efficiency (η_R) (Eq. 2), where $m_{released}$ and $m_{captured}$ are the absolute mass of released and captured water, respectively, and ω_{rel} is the mass of released water per unit mass of MOF ($\omega_{rel} \leq \omega_{cap}$). For a specific ω_{cap}, a maximum release efficiency can be achieved by using a MOF with high solar absorptivity, high thermal

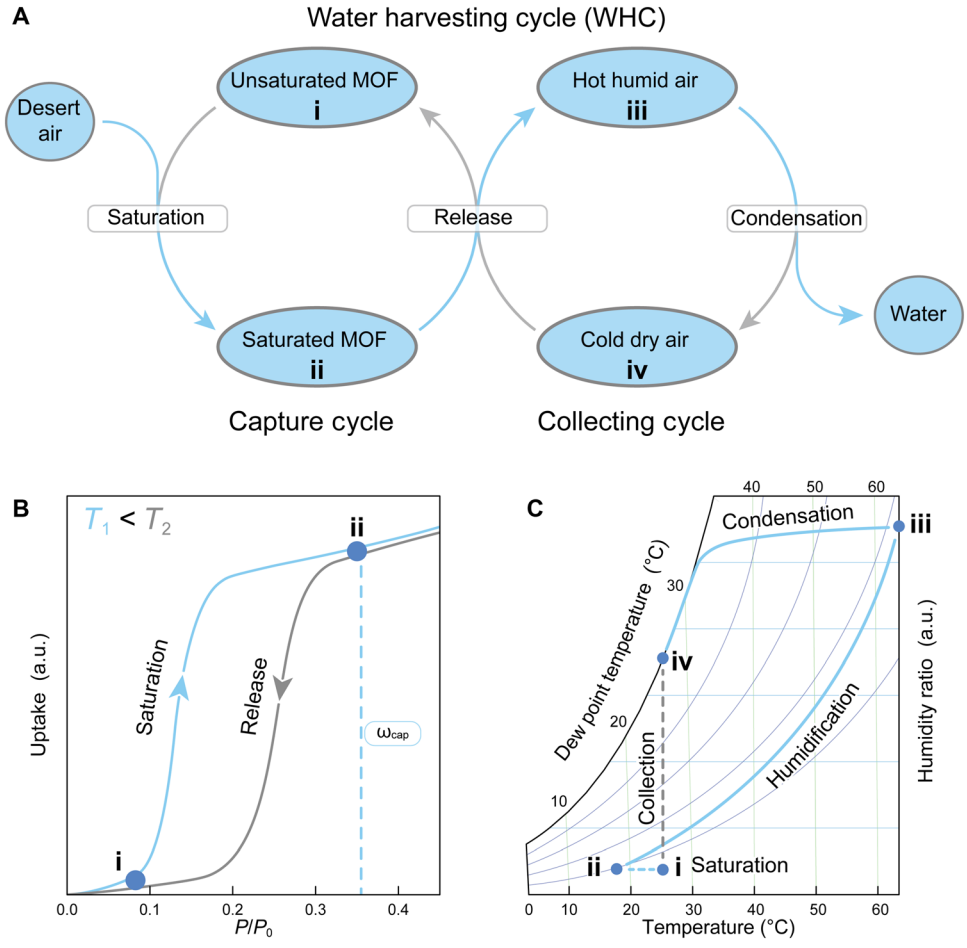

Fig. 1. WHC for practical water production under natural cooling and ambient sunlight. (**A**) The WHC is composed of the capture and collecting cycles. (**B**) The capture cycle is defined by the sorption isotherm of the MOF, and several prerequisites for high-performance water harvesting materials can be established therefrom. A type IV or type V isotherm with minimal or no hysteresis, a steep uptake below 25% RH, a high capture capacity (ω_{cap}) below 35% RH, and a significant shift of the inflection point for isotherms recorded at different temperatures are ideal. (**C**) The collecting cycle is defined by the psychrometric chart. During the release of captured water, the air is humidified and heated (ii→iii). Natural convection transports the hot humid air to the condenser, cooling it below its dew point (iii→iv). Concomitant condensation yields liquid water and dehumidified air. The collecting cycle can continue until the humidity ratio is too low for the dew point to be reached. a.u., arbitrary units.

conductivity, small heat capacity, and sorbent containment with maximized surface-to-volume ratio (see section S9). The release of water from the MOF at elevated temperatures should be significantly faster than the capture from desert air due to the limited time frame of the sunlight exposure

$$q_{H,min} > \omega_{cap} q_{st} \quad (1)$$

$$\eta_R = \frac{m_{released}}{m_{captured}} = \frac{\omega_{rel}}{\omega_{cap}} \quad (2)$$

The cooling energy required to condense the water vapor released from the MOF is spent on three processes: decreasing the temperature of the air and released water vapor ($q_{C,sensible}$), dewing ($q_{C,latent} = \omega_{cap} h_{fg}$), and dissipating due to heat loss ($q_{C,loss}$). Considering the large value of the specific heat of phase change (h_{fg}) (that is, enthalpy of condensation) for water, most of the cooling energy is spent on condensation rather than on sensible cooling ($q_{C,sensible} \ll q_{C,latent}$). A practical collecting cycle with adequate cooling capacity should satisfy the following criterion

$$q_{C,min} > \omega_{cap} h_{fg} \quad (3)$$

Inequality (Eq. 3) states that any design for atmospheric water production should consider a minimum $q_{C,min}$ that theoretically allows for the condensation of the entire amount of released water. The performance of the collecting cycle is evaluated by the collecting efficiency (η_C)

$$\eta_C = \frac{m_{collected}}{\omega_{rel} m_{MOF}} \quad (4)$$

where $m_{collected}$ and m_{MOF} are the mass of collected water and MOF, respectively. The main challenge for water production in a desert climate is to maintain the condenser temperature below the dew point

using only ambient cooling. This is possible by using an efficient condenser with a large cooling surface and enhanced convective heat and mass transfer. There is a theoretical maximum volume for the condenser beyond which the air saturation is not possible (see section S9).

The overall efficiency of the WHC is given by the harvesting efficiency (η_{WHC}) defined as

$$\eta_{WHC} = \frac{m_{collected}}{\omega_{cap} m_{MOF}} = \eta_R \eta_C \quad (5)$$

According to Eq. 5, highly efficient water production is only possible if the amount of water released from the MOF equals the captured amount ($\eta_R \rightarrow 1$) and if all the released water is condensed ($\eta_C \rightarrow 1$).

MOF-based water harvesting system

On the basis of this WHC and the considerations discussed above, a water harvesting system was designed initially using MOF-801 as the sorbent. MOF-801 was chosen for several reasons: (i) high hydrolytic stability, (ii) well-studied water sorption behavior, (iii) good cycling stability, (iv) low regeneration energy, and (v) a sorption isotherm that satisfies all mentioned prerequisites (*7*) for practical water production (Fig. 2A). Like most MOFs, MOF-801 shows low absorptivity in the infrared (IR) and near-IR region, low thermal conductivity (*16*), and high heat capacity (*17*), reducing direct heating using solar thermal energy. Hence, MOF-801 was blended with 33 weight % (wt %) of nonporous graphite (termed MOF-801/G) to enhance its thermophysical (*18*) and absorptive properties (see section S6). The water harvester consists of two main components: a water sorption unit that holds the MOF and the case that encloses it (Fig. 2B). The water sorption unit is designed to retain up to 2945 cm^3 of sorbent, equaling 1.2 kg of MOF-801 (1.65 kg of MOF-801/G) assuming a packing porosity of 0.7, the ideal value for moisture transfer (*15*). The geometry of the sorbent containment was chosen to facilitate a large surface-to-volume ratio (>0.5) of the MOF. In our original proof-of-concept design (*15*), we demonstrated that heating MOF-801 to 65°C at 10% RH is sufficient for water release; however, under these conditions, the condenser temperature should be below 20°C to achieve condensation. This significant temperature gradient is created by designing the water sorption unit to act as a thermal insulator, capable of maintaining a low condenser temperature while heating the MOF. The solar thermal incalescence of the water sorption unit itself was minimized by applying an IR reflective coating to all exposed surfaces. The cubic case has a cover and encloses the water sorption unit (Fig. 2B). The side walls of the case act as the condenser and provide surfaces for heat transfer with the surroundings. The case can be opened or closed for saturation during the night and release-condensation during the day. Finally, a reflector is attached to the cover to ensure that only the surface of the MOF is exposed to solar radiation. Temperature and humidity sensors are placed at the surface of the MOF powder and in the MOF powder, the bottom of the case, and the condenser. The data recorded with these sensors discussed below enable the calculations of the release, collecting, and WHC efficiencies.

Water production under controlled laboratory conditions

In a typical laboratory experiment, the sorbent was saturated overnight (RH, 30 to 50%; 18° to 25°C; 16.5 hours). After saturation, the case was sealed and exposed to artificial light (2700 K). Data were collected under low (558 W m^{-2}) and high radiant fluxes (792 W m^{-2}), representing the average solar irradiance over the course of 1 day and the peak solar irradiance in desert regions such as Arizona (33°N, 111°W), respectively. After 7.5 hours, the experiment was terminated, and liquid water was collected.

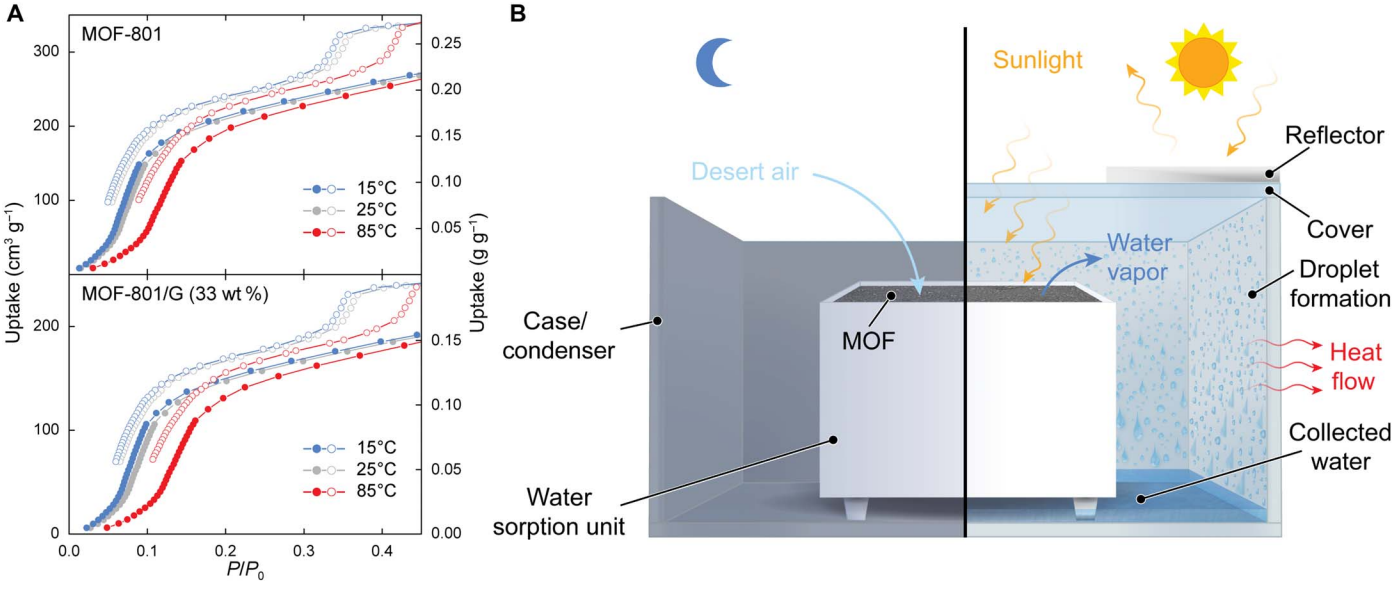

Fig. 2. Isotherms of MOF-801 and design of the MOF-based water harvester for water production from desert air. (**A**) Water sorption isotherms (adsorption, filled symbols; desorption, open symbols) of MOF-801 and MOF-801/G at 15°C (blue), 25°C (gray), and 85°C (red). In comparison to previously reported isotherms for MOF-801, a shift of the inflection point to higher relative pressures, a lower maximum capacity, and hysteresis were observed. These findings are related to a high degree of single crystallinity of the material (*23*). Blending MOF-801 with graphite led to a decrease of the gravimetric capacity corresponding to the added weight, while the general shape of the isotherm was fully retained. (**B**) Schematic of the water harvester consisting of a water sorption unit and a case. During the night, the cover of the case is opened, allowing the MOF to be saturated with moisture from desert air. During the day, the case is sealed to create a closed system. Humid hot air flows from the MOF to the condenser and is cooled down by heat rejection to the surroundings. When the dew point is reached, condensation occurs, and liquid water collects at the bottom of the case.

Initial experiments were performed using 1.65 kg of MOF-801/G under low and high radiant fluxes. While maintaining the condenser temperature at 20°C, the formation of fog on the condenser was observed after approximately 30 min (Fig. 3A). Formation of water droplets that subsequently coalesced into larger puddles occurred 2 to 3 hours into the experiment (see movies S1 to S4). Water production with low and high radiant fluxes yielded 25 and 56 g of water, respectively. Using the humidity and temperature measurements, the efficiencies were found to be η_R = 39 and 76%, η_C = 30 and 43%, and η_{WHC} = 12 and 33%, for low and high fluxes, respectively. The low collecting efficiency suggests a mismatch between the amount of released water and the cooling capacity of the condenser (that is, mismatch between the capture and collecting cycles). This issue was addressed by performing identical experiments using a half-loading of MOF-801/G (0.825 kg). Although a smaller amount of sorbent was used, larger quantities of water were collected (37 and 78 g of water for low and high fluxes, respectively), leading to increased efficiencies of η_R = 44 and 86%, η_C = 93 and 92%, and η_{WHC} = 41 and 79%, respectively. These major enhancements are attributed to improved water release ($\omega_{rel} \rightarrow \omega_{cap}$) due to a larger surface-to-volume ratio (~1) and faster energy transfer within the MOF, resulting in a longer effective condensation time (see section S9). While using even smaller amounts of MOF-801/G resulted in

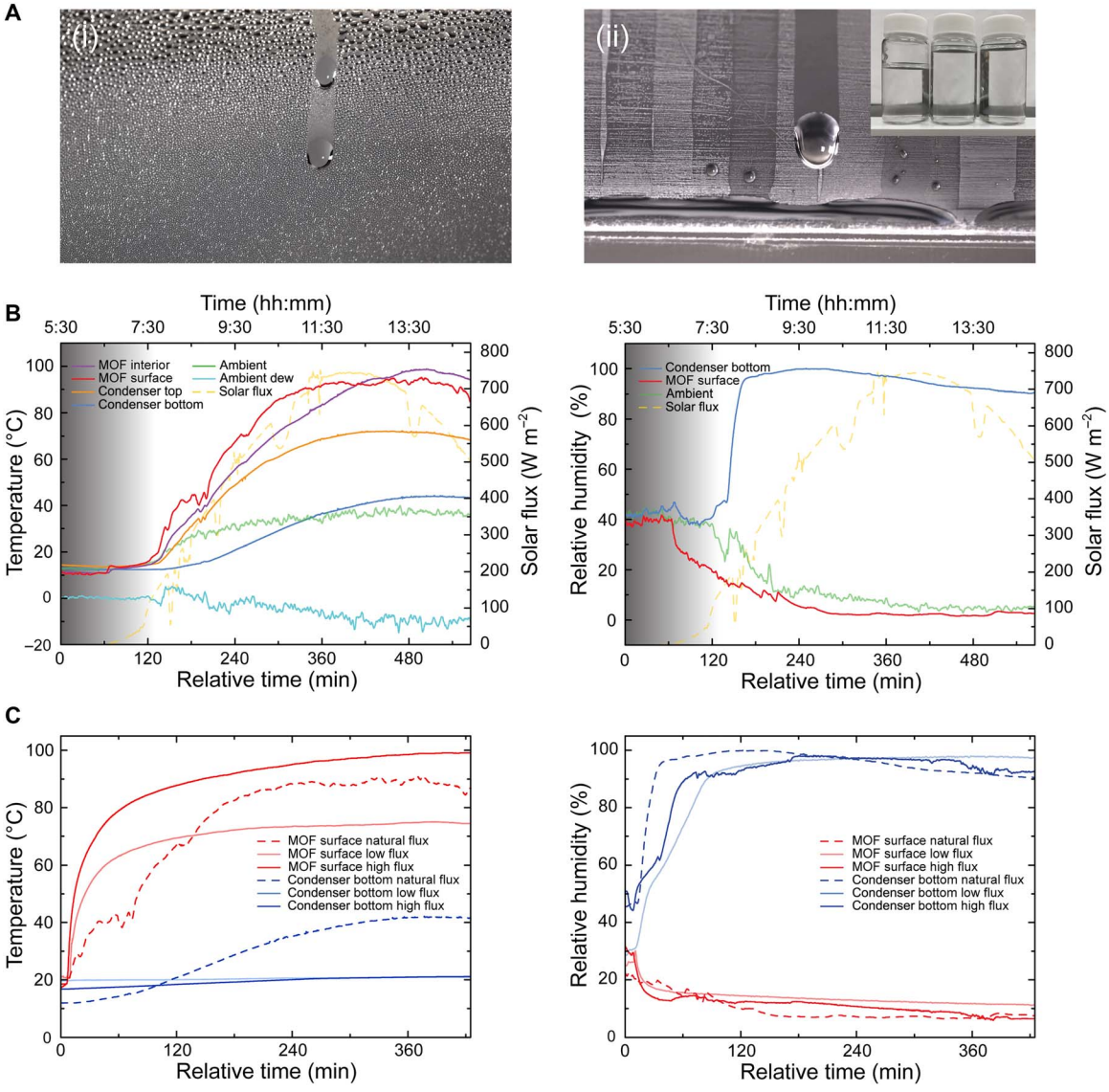

Fig. 3. Water production and temperature, RH, and solar flux profiles. (**A**) Photographs of the condenser showing (i) the formation of droplets (ii) flowing to make puddles (inset, water produced per day-and-night desert cycle). (**B**) Humidity and temperature profiles acquired during testing in the desert on 22 October 2017 in Scottsdale, AZ, USA. Temperature and humidity sensors were placed at different positions within the water harvester: at the bottom (orange) and top of the condenser (blue) and at the surface of (red) and in the MOF powder (magenta). The solar flux was recorded using a pyranometer mounted on the reflector. Ambient temperature and RH were monitored near the water harvester, and the ambient dew temperature (light blue) was calculated from these data. (**C**) Comparison of humidity and temperature profiles acquired under ambient solar flux during testing in the desert and under laboratory conditions using low (558 W m^{-2}) and high (792 W m^{-2}) fluxes. The origin represents when the complete surface of MOF-801/G was exposed to artificial or ambient solar radiation, for the laboratory experiments and the desert test, respectively.

further improvement of η_C and η_{WHC}, the absolute yield of water decreased. Therefore, using 0.825 kg of MOF-801/G provided us with a well-balanced water harvester with high values for η_R and η_C and a high nominal water yield that should be capable of operating under ambient cooling and on solar thermal energy solely (as in the desert). The chemical analysis of the produced water indicated the absence of contaminations originating from dissolution of the MOF for all experiments (see section S11).

Water production in desert conditions

We then transferred this device to Scottsdale, AZ, in late October 2017 to study its performance under desert conditions (as low as 5% RH at 35° to 40°C during the day and up to 40% RH at 10° to 15°C during the night) and to validate the water harvesting principles discussed above. Under these operating conditions, the dew point is found to be at subzero temperatures, rendering refrigeration-based water production infeasible (Fig. 3B) (*15*, *19*). Initial experiments using the water harvester under desert conditions, however, were unsuccessful and did not yield liquid water. The high ambient temperatures during the day resulted in markedly increased condenser temperatures (42°C), lowering the temperature difference between the MOF and the condenser to approximately 30°C and hampering condensation (RH < 88% at the condenser). To circumvent warming of the condenser by heat transfer from the surroundings, we used exterior insulation (soil) with a high heat capacity and low thermal conductivity (*20*). This modification facilitated a significant reduction of the condenser temperature by 10°C and resulted in 94% RH at the condenser. Consequently, the formation of fog was observed, but the temperature difference between the MOF and the condenser (40°C) was still not sufficient to reach the higher humidity ratio required to condense larger quantities of water. More solar energy was needed to further increase the temperature difference between the MOF and the condenser. During October, the altitude of the sun at Scottsdale [degrees/minutes/seconds (DMS) latitude, 33°30′4.7664″N; DMS longitude, 111°55′31.000″W] varies between 20° in the morning and late afternoon (9 a.m. and 4 p.m.) and 45° at midday (*21*). Thus, the water harvester was mounted on a stand and tilted by 37° to maximize the solar energy absorbed by the MOF. With this modification, MOF temperatures like those recorded under laboratory conditions could be reproduced, and indeed, after 7 hours, liquid water was collected. More absorbed solar energy allowed for faster water release, as indicated by an instantaneous rise of RH at the condenser, which, in combination with the delayed heating of the condenser itself, facilitated condensation (Fig. 3B). Using 0.825 kg of MOF-801/G, 55 g of water was collected, a value between those obtained under laboratory conditions for low flux (37 g) and high flux (78 g). This is in agreement with the corresponding temperature and RH profiles, as shown in Fig. 3C.

Highly efficient water production with a next-generation MOF

To bring this development closer to practical use, we sought to make MOFs with enhanced water sorption properties potentially meeting the specification of industrial large-scale production. We developed the synthesis of the next-generation material MOF-303 [Al(OH)(HPDC); HPDC, 1*H*-pyrazole-3,5-dicarboxylate], using aluminum instead of zirconium as the metal and using water instead of organic solvents. It has a new structure based on the **xhh** topology and is built from infinite Al(OH)(-COO)$_2$ secondary building units (SBUs) linked through HPDC linkers (Fig. 4A) (*22*). The structure of MOF-303

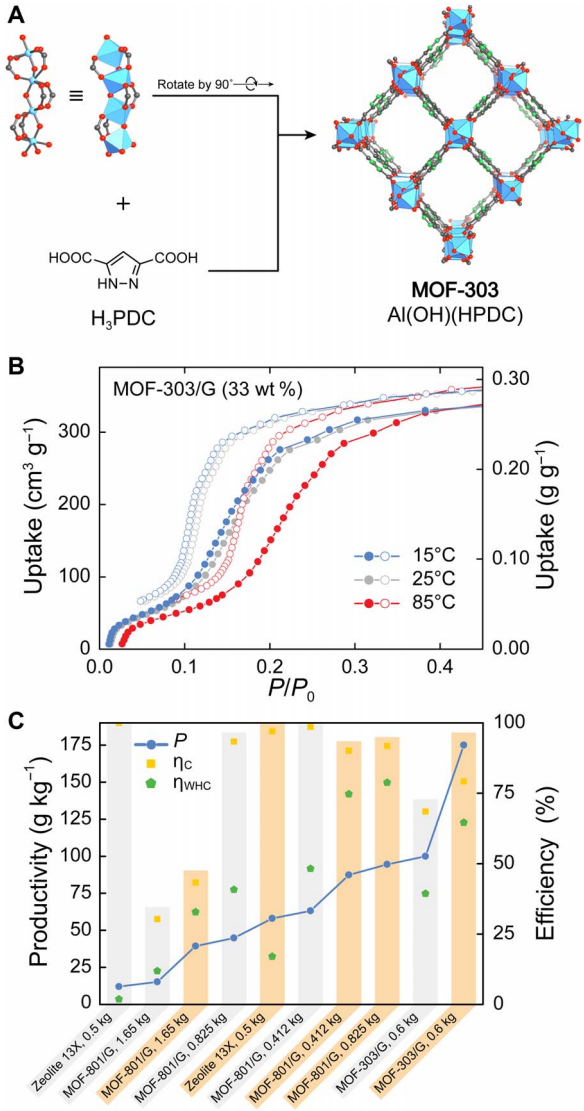

Fig. 4. Next-generation MOF with increased productivity. (**A**) Crystal structure of MOF-303 built from rod-like Al(OH)(-COO)$_2$ SBUs linked by HPDC linkers into an extended framework structure (**xhh** topology) with a 1D pore system. Gray, C; green, N; red, O; blue polyhedra, Al. (**B**) Water sorption isotherms for MOF-303/G at 15°C (blue), 25°C (gray), and 85°C (red). (**C**) Comparison of parameters defining the efficiency and productivity of the water harvester. Gray and orange bars represent measurements under low and high fluxes, respectively.

features hydrophilic one-dimensional (1D) pores with a 6 Å diameter and a free pore volume of 0.54 cm^3 g^{-1}, facilitating a large maximum water capture capacity of 0.48 g g^{-1}. The water sorption isotherm satisfies all prerequisites for a high-performance water harvesting material outlined earlier: The type IV isotherm has an inflection point at P/P_0 = 0.15, a plateau is reached at P/P_0 = 0.3, and good temperature response and minimal hysteresis are observed (Fig. 4B). In addition, high hydrolytic stability was confirmed by carrying out 150 adsorption-desorption cycles without measurable degradation of the material (see fig. S24). Despite the larger ω_{cap} for MOF-303, both criteria are satisfied for $q_{H,min}$ and $q_{C,min}$ for operating conditions found in Arizona (RH at night, ambient temperature, and solar flux), thus making the present water harvester suitable for MOF-303. In a manner akin to that described

for MOF-801, the thermophysical and absorptive properties of MOF-303 were enhanced by blending it with 33 wt % of nonporous graphite (termed MOF-303/G; see section S6). MOF-303/G was tested under the same laboratory conditions described above and found to give a marked increase of 114% in water production (see section S9).

Ultimately, the performance of a sorbent according to the WHC is defined by the productivity P (in grams per kilogram)

$$P = \frac{m_{\text{collected}}}{m_{\text{sorbent}}} \quad (6)$$

where m_{sorbent} is the amount of sorbent used (in kilograms). This parameter is useful in comparing the performance of various materials under identical conditions within the same water harvester. Zeolite 13X was chosen as a reference because it is a common microporous desiccant with a pore size and pore volume similar to those of MOF-801 and MOF-303. Figure 4C shows the comparison of productivities calculated for zeolite 13X, MOF-801/G, and MOF-303/G. This comparison is striking evidence that the unique water sorption behavior of MOFs is key to water production from desert air under ambient cooling and solely driven by solar thermal energy. The ultrahigh productivity of MOF-303/G of up to 175 grams water per kilogram of MOF/G is encouraging in achieving practical water production from desert air.

CONCLUSION

The discovery of the criteria governing energy, materials, and air requirements for practical production of water from desert air as outlined in this report should be applicable to various regions of the world. The development of the next-generation MOF-303 highlights the prospect of MOFs with respect to this application arising from the flexibility of design and synthesis of these framework materials. This, in combination with the design considerations outlined in this report, brings water production in desert climates one step closer to practical applications.

MATERIALS AND METHODS

Synthesis of MOF materials

MOF-801 [$Zr_6O_4(OH)_4$(fumarate)$_6$] was prepared by dissolving 5.8 g/50 mmol of fumaric acid and 16 g/50 mmol of zirconyl chloride octahydrate ($ZrOCl_2{\cdot}8H_2O$) in a mixture of 200 ml of *N*,*N*′-dimethylformamide (DMF) and 70 ml of formic acid in a 500-ml glass screw-capped jar. The mixture was subsequently heated at 130°C overnight, and the white precipitate was separated by filtration (yield, ~10 g). The precipitates of five reactions were combined, washed three times daily with 500 ml of DMF for 3 days and then three times daily with 500 ml of methanol for 3 days, and subsequently dried in air. The air-dried sample was then transferred to a vacuum chamber, evacuated at room temperature for 5 hours, followed by evacuation at 70°C for 12 hours and 150°C for 48 hours. The activated product of 140 jars was combined and dried at 160°C for 10 days.

MOF-303 [Al(OH)(HPDC)(H_2O)] was prepared by dissolving 10.4 g/43.08 mmol of aluminum chloride hexahydrate ($AlCl_3{\cdot}6H_2O$) and 7.5 g/43.08 mmol of 3,5-pyrazoledicarboxylic acid monohydrate ($H_3PDC{\cdot}H_2O$) in 720 ml of water in a 1-liter glass screw-capped jar. We added 2.6 g/65 mmol of NaOH dropwise in 30 ml of water to the above mixture under stirring. Subsequently, the jar was sealed and heated at 100°C for 24 hours, and the resulting white precipitate was separated by filtration (yield, 3.0 g). The precipitate was washed three times daily with water for 3 days and then three times daily with methanol for 3 days and was then filtered and dried in air. The air-dried sample was transferred into a vacuum chamber and evacuated until the pressure dropped below 1 kPa, followed by evacuation at 100°C for 24 hours and at 150°C for another 48 hours. The activated product of 150 jars was combined and dried at 160°C for 10 days.

MOF-graphite mixtures with enhanced thermophysical and spectroscopic properties were prepared by mixing activated MOF with 33 wt % of nonporous graphite powder until a homogeneous color was observed. The resulting mixtures were further characterized in terms of crystallinity, powder density, porosity, and water uptake properties without any additional activation.

Characterization and chemical analysis

Powder x-ray diffraction (PXRD) patterns of MOF-801, MOF-801/G, MOF-303, and MOF-303/G were recorded with a Bruker D8 ADVANCE diffractometer (Göbel-mirror monochromated Cu Kα1 radiation, λ = 1.54056 Å). Typically, data were collected between 3° and 50° with a step width of 0.01 and a total data collection time of 30 min.

Nitrogen gas adsorption isotherms were recorded on a Quantachrome QUADRASORB-SI volumetric gas adsorption analyzer at 77 K. Volumetric water adsorption isotherms and stability tests were measured on a BEL Japan BELSORP-aqua3, for which the water (analyte) was degassed through three freeze-pump-thaw cycles. Helium gas was used to estimate the dead space for both gas and water adsorption measurements. The framework density of all MOF and MOF/G samples was measured using a pycnometer (Ultrapyc 1200e, Quantachrome). Ultrahigh-purity gases (He and N_2; Praxair, 99.999% purity) were used for all experiments.

Attenuated total reflectance Fourier transform infrared (ATR-FTIR) spectra were recorded on a Bruker ALPHA Platinum ATR-FTIR spectrometer. Diffuse reflectance spectra between 285 and 2500 nm were recorded on a Varian Cary 5000 spectrometer. Absorption spectra between 285 and 3000 nm were recorded using a Shimadzu UV-3600 equipped with a double monochromator having a wavelength range of 185 to 3300 nm. A photomultiplier tube (ultraviolet and visible region) and an InGaAs and cooled PbS detector (long-wavelength detection) were used.

Thermogravimetric analysis (TGA) measurements were performed on a TA Instruments SDT-Q600 series thermal gravimetric analyzer. Gases were humidified by bubbling dry air through a 2-liter bubbler humidifier, and both humidity and temperature were monitored using high-accuracy thermocouples and humidity sensors upstream of the TGA chamber (see section S6).

The morphology and elemental distribution of all MOF and MOF/G samples were examined by scanning electron microscopy (SEM) and energy-dispersive x-ray spectroscopy (FEI Quanta 3D scanning electron microscope, 10-kV accelerating voltage). Water samples were examined using nuclear magnetic resonance (NMR) spectroscopy (Bruker DRX-500) and inductively coupled plasma atomic emission spectroscopy (Optima 7000 DV, PerkinElmer).

The thermal response of all materials was measured using a homemade setup (S7) consisting of an insulation cell made of extruded polystyrene foam with a fast-response T-type thermocouple (Neoflon PFA, American Wire Gauge 40, OMEGA Engineering) installed at the bottom of the cell. An incandescent lamp (150 W) was placed 60 cm above the cell to ensure the flux of 1000 ± 30 W m^{-2}, and the

cell temperature was equilibrated with the surroundings before flux exposure (25° ± 0.5°C).

Device fabrication

The water sorption unit was composed of four rectangular walls made from transparent poly(methyl methacrylate) (PMMA) pieces (18.25″ × 8.00″ × 0.25″) installed onto a square PMMA plate (18.50″ × 18.50″ × 0.25″). A sorbent container (16″ × 16″ × 1″ held by a 2.50″ wide frame) made of 0.25″ thick PMMA was glued to the upper side of the side walls, creating a sealed compartment that was packed with extruded polystyrene foam (Owens Corning). The sorbent container was coated with a high solar absorptivity black coating (Pyromark 1200 high-temperature paint, purchased from LA-CO) to enhance the solar absorbance. All other exposed surfaces of the water sorption unit were treated with a high reflectivity coating in the infrared region (2X paint, Rust-Oleum).

The case consists of a tub and a cover made from 0.25″ PMMA. The tub was constructed from four square side walls (22″ × 22″) connected to a support plat (22″ × 22″, bottom) and a 2″ wide frame support (24″ outer length, top). A cover (22″ × 22″) was screwed to the support frame using 12 screws, and the joint was sealed using a Teflon gasket. A solar reflector, made from 1″ thick extruded polystyrene foam covered with aluminum tape (3M Aluminum Foil Tape 425) with a 21″ × 21″ square opening was positioned on the cover. All PMMA used for the construction of the water sorption unit, cover, and case was purchased from McMaster-Carr and cut using a Universal Laser Cut ILS12.75 with a materials processing envelope of 48″ × 24″ × 12″. The individual PMMA pieces were connected using acrylic cement (Scigrip). In the laboratory experiment, the case was placed on a T-slotted aluminum frame measuring 2′ × 2′ × 3′ ($1\,^1/_2$″ high × $1\,^1/_2$″ wide; Single Rail, Silver). In desert experiments, the case was insulated using an exterior wooden box (3′ × 3′ × 1′) filled with soil (packing porosity of ~0.65).

Data acquisition: Temperature and humidity measurements

In all the experiments, temperature and humidity readings were acquired using a National Instruments data acquisition system (cDAQ-9174) with a NI 9205 32-Channel analog input and NI 9214 16-Ch Isothermal TC modules, respectively. All data were recorded using LabView 2016. Temperature and humidity measurements were taken at various locations inside the case (at the top and bottom of the condenser, inside and at the surface of the sorbent powder, and at the exterior side wall of the case) and outside of the case (ambient temperature and humidity).

The RH was measured with integrated fast-response (response time, <4 s) circuit sensors (Honeywell HIH-4021) with thermoset polymer capacitive sensing elements. The humidity sensors were calibrated within a range of RH (5% < RH < 90% in 5% RH increments and at T = 25°C) using a HygroCal100 humidity generator (Michell Inc.). The HygroCal100 is equipped with seven built-in HygroSmart HS3 capacitive humidity sensors (±0.8% accuracy) enabling humidity uniformity (less than ±0.5%) across the humidity chamber. An external standard reference precision dew-point meter (Optidew Vision precision, Michell Inc.) with ±0.2°C uncertainty in dew temperature was used to zero the bias error of the HygroCal100. Fifty voltage readings with a sampling frequency of 30 s were recorded at each humidity level, while the hysteresis effects were quantified through a loop of increasing (5 to 90%) and decreasing (95 to 5%) humidity. A linear regression curve (coefficient of determination of >0.99 with 95% confidence bounds) was applied to convert sensor voltage output (0.5 to 3.0 V) to RH (0 to 100%). The total uncertainty of the RH readings was determined to be less than 1%. The detailed uncertainty analysis and the corresponding regression curve are given in section S8.

T-type thermocouples (Neoflon PFA, American Wire Gauge 40, OMEGA Engineering) were calibrated within the range of 15° to 105°C in 5°C increments using a Hart Scientific 9103 dry-well calibrator with an accuracy of ±0.25°C. Forty readings with a sampling rate of 5 s were taken at each reference temperature, and hysteresis effects were determined through an increasing-decreasing temperature loop. A linear regression curve was used for data reduction (coefficient of determination of >0.99 with 95% confidence bounds), giving a bias error of ±0.04°C. The total uncertainty in the temperature readings was found to be less than ±0.25°C. The detailed uncertainty analysis with the regression curve is given in section S8.

SUPPLEMENTARY MATERIALS

Supplementary material for this article is available at http://advances.sciencemag.org/cgi/content/full/4/6/eaat3198/DC1

section S1. Materials and analytical techniques for MOF synthesis and analysis
section S2. MOF-801 synthesis and characterization
section S3. MOF-801/G preparation and characterization
section S4. MOF-303 synthesis and characterization
section S5. MOF-303/G preparation and characterization
section S6. Comparison of sorbents
section S7. Water harvester
section S8. Data acquisition and sensors
section S9. WHC under laboratory conditions
section S10. Harvesting experiments at Scottsdale, AZ, under desert conditions
section S11. Chemical analysis of collected water samples and MOF chemical stability
section S12. Movies of the water production experiment
fig. S1. PXRD pattern of activated MOF-801.
fig. S2. SEM image of activated MOF-801.
fig. S3. SEM and EDS images of MOF-801.
fig. S4. N_2 isotherm of activated MOF-801 recorded at 77 K.
fig. S5. Water sorption isotherms of pre–scaled-up MOF-801 sample (black, this work), MOF-801-P (red), and MOF-801-SC (blue) (*7*).
fig. S6. Water sorption isotherms of pre–scaled-up MOF-801 recorded at different temperatures.
fig. S7. Characteristic curves for activated pre–scaled-up MOF-801 determined using Eqs. 2 and 3 based on the sorption isotherms measured at different temperatures.
fig. S8. Isosteric heat of adsorption (black) and water sorption isotherm at 25°C (red) for activated MOF-801.
fig. S9. Experimental water sorption isotherm for activated scaled-up MOF-801 recorded at 25°C and calculated water sorption isotherms at 15 and 85°C.
fig. S10. PXRD pattern of the graphite sample.
fig. S11. PXRD pattern of activated sample of MOF-801/G.
fig. S12. SEM and EDS images of MOF-801/G.
fig. S13. N_2 isotherm of the activated MOF-801/G recorded at 77 K.
fig. S14. Experimental water sorption isotherm for MOF-801/G at 25°C and calculated water sorption isotherms at 15° and 85°C.
fig. S15. Comparison of water sorption isotherms for scaled-up MOF-801 and MOF-801/G at 25°C.
fig. S16. Asymmetric unit in the single-crystal structure of MOF-303 (atoms are shown isotropically).
fig. S17. PXRD pattern of activated MOF-303.
fig. S18. SEM image of activated MOF-303.
fig. S19. SEM and EDS images of MOF-303.
fig. S20. N_2 isotherm of activated scaled-up MOF-303 at 77 K.
fig. S21. Water sorption isotherm of pre–scaled-up activated MOF-303 recorded at 25°C.
fig. S22. Cycling experiment of MOF-303.
fig. S23. Water sorption isotherms of activated scaled-up MOF-303 at different temperatures.
fig. S24. One hundred fifty cycles of RH swing cycling of scaled-up activated MOF-303 at 25°C in a TGA.
fig. S25. Characteristic curves determined using Eqs. 2 and 3 based on sorption isotherms for MOF-303 measured at different temperatures.
fig. S26. Isosteric heat of adsorption (black) versus water sorption isotherm at 25°C (red) for activated MOF-303.

REFERENCES AND NOTES

1. P. H. Gleick, *Water in Crisis: A Guide to the World's Fresh Water Resources* (Oxford Univ. Press, 1993).
2. K.-C. Park, S. S. Chhatre, S. Srinivasan, R. E. Cohen, G. H. McKinley, Optimal design of permeable fiber network structures for fog harvesting. *Langmuir* **29**, 13269–13277 (2013).
3. O. Klemm, R. S. Schemenauer, A. Lummerich, P. Cereceda, V. Marzol, D. Corell, J. van Heerden, D. Reinhard, T. Gherezghiher, J. Olivier, P. Osses, J. Sarsour, E. Frost, M. J. Estrela, J. A. Valiente, G. M. Fessehaye, Fog as a fresh-water resource: Overview and perspectives. *Ambio* **41**, 221–234 (2012).
4. R. S. Schemenauer, P. Cereceda, A proposed standard fog collector for use in high-elevation regions. *J. Appl. Meteorol. Climatol.* **33**, 1313–1322 (1994).
5. M. Muselli, D. Beysens, J. Marcillat, I. Milimouk, T. Nilsson, A. Louche, Dew water collector for potable water in Ajaccio (Corsica Island, France). *Atmos. Res.* **64**, 297–312 (2002).
6. R. V. Wahlgren, Atmospheric water vapour processor designs for potable water production: A review. *Water Res.* **35**, 1–22 (2001).
7. H. Furukawa, F. Gándara, Y.-B. Zhang, J. Jiang, W. L. Queen, M. R. Hudson, O. M. Yaghi, Water adsorption in porous metal–organic frameworks and related materials. *J. Am. Chem. Soc.* **136**, 4369–4381 (2014).
8. SunToWater Technologies LLC, *Two-stage desiccant system* (2508 Highlander Way, 2017); http://suntowater.com/.
9. D. Fröhlich, S. K. Henninger, C. Janiak, Multicycle water vapour stability of microporous breathing MOF aluminium isophthalate CAU-10-H. *Dalton Trans.* **43**, 15300–15304 (2014).

10. G. E. Cmarik, M. Kim, S. M. Cohen, K. S. Walton, Tuning the adsorption properties of UiO-66 via ligand functionalization. *Langmuir* **28**, 15606–15613 (2012).
11. A. J. Rieth, S. Yang, E. N. Wang, M. Dincă, Record atmospheric fresh water capture and heat transfer with a material operating at the water uptake reversibility limit. *ACS Cent. Sci.* **3**, 668–672 (2017).
12. J. Canivet, J. Bonnefoy, C. Daniel, A. Legrand, B. Coasne, D. Farrusseng, Structure–property relationships of water adsorption in metal–organic frameworks. *New J. Chem.* **38**, 3102–3111 (2014).
13. V. Bon, I. Senkovska, I. A. Baburin, S. Kaskel, Zr- and Hf-based metal–organic frameworks: Tracking down the polymorphism. *Cryst. Growth Des.* **13**, 1231–1237 (2013).
14. A. Cadiau, J. S. Lee, D. Damasceno Borges, P. Fabry, T. Devic, M. T. Wharmby, C. Martineau, D. Foucher, F. Taulelle, C.-H. Jun, Y. K. Hwang, N. Stock, M. F. De Lange, F. Kapteijn, J. Gascon, G. Maurin, J.-S. Chang, C. Serre, Design of hydrophilic metal organic framework water adsorbents for heat reallocation. *Adv. Mater.* **27**, 4775–4780 (2015).
15. H. Kim, S. Yang, S. R. Rao, S. Narayanan, E. A. Kapustin, H. Furukawa, A. S. Umans, O. M. Yaghi, E. N. Wang, Water harvesting from air with metal-organic frameworks powered by natural sunlight. *Science* **356**, 430–434 (2017).
16. B. L. Huang, Z. Ni, A. Millward, A. J. H. McGaughey, C. Uher, M. Kaviany, O. Yaghi, Thermal conductivity of a metal-organic framework (MOF-5): Part II. Measurement. *Int. J. Heat Mass Transf.* **50**, 405–411 (2007).
17. F. A. Kloutse, R. Zacharia, D. Cossement, R. Chahine, Specific heat capacities of MOF-5, Cu-BTC, Fe-BTC, MOF-177 and MIL-53 (Al) over wide temperature ranges: Measurements and application of empirical group contribution method. *Microporous. Mesoporous. Mater.* **217**, 1–5 (2015).
18. S. Yang, X. Huang, G. Chen, E. N. Wang, Three-dimensional graphene enhanced heat conduction of porous crystals. *J. Porous Mater.* **23**, 1647–1652 (2016).
19. E. D. Wikramanayake, O. Ozkan, V. Bahadur, Landfill gas-powered atmospheric water harvesting for oilfield operations in the United States. *Energy* **138**, 647–658 (2017).
20. O. T. Farouki, *Thermal Properties of Soil* (U.S. Army Corps of Engineers, Cold Regions Research and Engineering Laboratory, 1986).
21. *2009 ASHRAE Handbook-Fundamentals* (American Society of Heating, Refrigerating and Air-Conditioning Engineers Inc, ed. IP, 2009).
22. M. O'Keeffe, M. A. Peskov, S. J. Ramsden, O. M. Yaghi, The Reticular Chemistry Structure Resource (RCSR) database of, and symbols for, crystal nets. *Acc. Chem. Res.* **41**, 1782–1789 (2008).
23. P. Ghosh, Y. J. Colón, R. Q. Snurr, Water adsorption in UiO-66: the importance of defects. *Chem. Commun.* **50**, 11329–11331 (2014).
24. M. F. de Lange, K. J. F. M. Verouden, T. J. H. Vlugt, J. Gascon, F. Kapteijn, Adsorption-driven heat pumps: The potential of metal–organic frameworks. *Chem. Rev.* **115**, 12205–12250 (2015).
25. Bruker, APEX2, Bruker AXS Inc., Madison, Wisconsin, USA (2010).
26. G. M. Sheldrick, A short history of SHELX. *Acta Crystallogr. A Found. Adv.* **64**, 112–122 (2008).
27. Discovery Studio Modeling Environment, Release 7.0 (Accelrys Software Inc., 2006).
28. Laboratory Virtual Instrument Engineering Workbench (LabVIEW), Release 2016 (National Instruments, 2016).
29. Matrix Laboratory (MATLAB), Release 2017a (The MathWorks Inc., 2017).
30. E. S. Domalski, E. D. Hearing, Condensed phase heat capacity data, in *NIST Chemistry WebBook, NIST Standard Reference Database Number 69*, P. J. Linstrom, G. Mallard, Eds. (National Institute of Standards and Technology, 2018).
31. K. G. T. Hollands, G. D. Raithby, L. Konicek, Correlation equations for free convection heat transfer in horizontal layers of air and water. *Int. J. Heat Mass Transf.* **18**, 879–884 (1975).
32. A. Giri, D. Bhuyan, B. Das, A study of mixed convection heat transfer with condensation from a parallel plate channel. *Int. J. Therm. Sci.* **98**, 165–178 (2015).

Acknowledgments: We thank B. Rungtaweevoranit, Y. Liu, J. Baek, C. Hong, S. Lyle, C. Trickett, T. O'Donnell, S. McNally, S. Alahmadi, and P. Kang for helpful discussions and assistance and B. Landon and J. Landon of Tempe, AZ, for allowing us to use their home for the initial desert experiments. O.M.Y. acknowledges the collaboration, valuable input, and support of Prince Turki bin Saud bin Mohammed Al-Saud (president of KACST). **Funding:** We are grateful to the support of Baden Aniline and Soda Factory–Ludwigshafen, Germany, for synthesis and characterization of compounds and King Abdulaziz City of Science and Technology, Saudi Arabia, for water adsorption studies. M.J.K. is grateful for financial support through the German Research Foundation (DFG; KA 4484/1-1). P.J.W. thanks the NSF and the Berkeley Center for Green Chemistry for support via the Systems Approach to Green Energy Integrative Graduate Education and Research Traineeship (1144885). **Author contributions:** F.F., M.J.K., and E.A.K. designed the prototype, set up the experimental procedures, conducted the laboratory and desert experiments, and processed and analyzed the experimental data. P.J.W. and J.Y. prepared MOF samples. F.F., M.J.K., E.A.K., and O.M.Y. prepared the manuscript. All authors contributed to the final version. O.M.Y. conceived the idea and led the project. **Competing interests:** The authors declare that they have no competing interests. **Data and materials availability:** All data needed to evaluate the conclusions in the paper are present in the paper and/or the Supplementary Materials. Additional data related to this paper may be requested from the authors.

Submitted 15 February 2018
Accepted 24 April 2018
Published 8 June 2018
10.1126/sciadv.aat3198

Citation: F. Fathieh, M. J. Kalmutzki, E. A. Kapustin, P. J. Waller, J. Yang, O. M. Yaghi, Practical water production from desert air. *Sci. Adv.* **4**, eaat3198 (2018).

ScienceAdvances

Practical water production from desert air

Farhad Fathieh, Markus J. Kalmutzki, Eugene A. Kapustin, Peter J. Waller, Jingjing Yang and Omar M. Yaghi

Sci Adv **4** (6), eaat3198.
DOI: 10.1126/sciadv.aat3198